Amyloid-β precursor protein processing and oxidative stress are altered in human iPSC-derived neuron and astrocyte co-cultures carrying presenillin-1 gene mutations following spontaneous differentiation

Elsworthy, Richard; King, Marianne; Grainger, Alastair; Fisher, Emily; Crowe, James; Alqattan, Sarah; Ludlam, Adele; Hill, Eric J; Aldred, Sarah

DOI:
10.1016/j.mcn.2021.103631

Document Version
Peer reviewed version

Citation for published version (Harvard):
Elsworthy, R, King, M, Grainger, A, Fisher, E, Crowe, J, Alqattan, S, Ludlam, A, Hill, EJ & Aldred, S 2021, 'Amyloid-β precursor protein processing and oxidative stress are altered in human iPSC-derived neuron and astrocyte co-cultures carrying presenillin-1 gene mutations following spontaneous differentiation', *Molecular and Cellular Neuroscience*, vol. 114, 103631. https://doi.org/10.1016/j.mcn.2021.103631

Amyloid-β Precursor Protein Processing and Oxidative Stress are Altered in Human iPSC-Derived Neuron and Astrocyte Co-Cultures Carrying Presenillin-1 Gene Mutations Following Spontaneous Differentiation

Richard J Elsworthy[1,3], Marianne C King[2], Alastair Grainger[2], Emily Fisher[1], James A Crowe[2], Sarah Alqattan[2], Adele Ludlam[2], Dr Eric J Hill[2]*, Dr Sarah Aldred[1,3]*

[1]School of Sport, Exercise and Rehabilitation Sciences, College of Life and Environmental Sciences, University of Birmingham, Birmingham, UK.

[2]Aston Research Centre for Healthy Ageing (ARCHA), School of Life and Health Sciences, Aston University, Birmingham, UK.

[3]Centre for Human Brain Health (CHBH), University of Birmingham, Edgbaston, Birmingham, UK

* Corresponding Authors:

Dr Sarah Aldred - s.aldred.1@bham.ac.uk

Dr Eric J Hill - e.j.hill@aston.ac.uk

Abstract

INTRODUCTION: Presenilin-1 (PSEN1) gene mutations are the most common cause of familial Alzheimer's disease (fAD) and are known to interfere with activity of the membrane imbedded γ-secretase complex. PSEN1 mutations have been shown to shift Amyloid-β precursor protein (AβPP) processing toward amyloid-β (Aβ) 1-42 production. However, less is known about whether PSEN1 mutations may alter the activity of enzymes such as ADAM10, involved with non-amyloidogenic AβPP processing, and markers of oxidative stress.

MATERIALS AND METHODS: Control and PSEN1 mutation (L286V and R278I) Human Neural Stem Cells were spontaneously differentiated into neuron and astrocyte co-cultures. Cell lysates and culture media were collected and stored at -80°C until further analysis. ADAM10 protein expression, the ratio of AβPP forms and Aβ1-42/40 were assessed. In addition, cellular redox status was quantified.

RESULTS: The ratio of AβPP isoforms (130:110kDa) was significantly reduced in neuron and astrocyte co-cultures carrying PSEN1 gene mutations compared to control, and mature ADAM10 expression was lower in these cells. s*A*βPP-α was also significantly reduced in L286V mutation, but not in the R278I mutation cells. Both Aβ1-40 and Aβ1-42 were increased in conditioned cell media from L286V cells, however, this was not matched in R278I cells. The Aβ1-42:40 ratio was significantly elevated in R278I cells. Markers of protein carbonylation and lipid peroxidation were altered in both l286V and R278I mutations. Antioxidant status was significantly lower in R278I cells compared to control cells.

CONCLUSIONS: This data provides evidence that the PSEN1 mutations L286V and R278I significantly alter protein expression associated with AβPP processing and cellular redox status. In addition, this study highlights the potential for iPSC-derived neuron and astrocyte co-cultures to be used as an early human model of fAD.

Keywords: Alzheimer's Disease, Amyloid-β, Presenilin-1, ADAM10, iPSCs, Oxidative stress.

Introduction

Advances in stem cell biology have enabled the unique ability to manipulate the human central nervous system (CNS), allowing the exploration of regenerative medicine and disease modelling with greater relevance to human tissue than previously possible (Shi et al 2012). By reprogramming human somatic cells back to a state of induced pluripotency (Takahashi & Yamanaka 2006) it is possible to direct differentiation towards neural precursor cells and ultimately into functional neuron and astrocytic co-cultures that are more representative of human brain tissue than currently used models (Gunhanlar et al 2018, Hill et al 2016). The potential to probe human derived CNS networks is of great interest for developing our understanding of, and exploring the effect of interventions on, the pathological processes underlying Alzheimer's disease (AD). The presentation of key biochemical features, including altered Amyloid-β Precursor Protein (AβPP) processing, hyperphosphorylated tau-protein and increased oxidative stress in induced pluripotent stem cell (iPSC) neural networks derived from people with AD suggests this model may be a useful tool in studying the progression of AD (Hossini et al 2015, Kondo et al 2013). Crucially, it has been shown that tissue that has been reprogrammed from people with AD into cortical neurons, exhibited phenotypes that are observed '*in vivo*' (Israel et al 2012).

The *PSEN1* gene encodes for the protein Presenilin-1 (PS1). Mutations in this gene are the most common cause of familial AD and are known to interfere with activity of the membrane imbedded γ-secretase complex (Kelleher & Shen 2017). γ-secretase is comprised of four subunits (Lu et al 2014) and has an important role in cellular functions, as it cleaves substrates such as Notch and the AβPP. As PS1 forms the catalytic subunit of γ-secretase, mutations in the PSEN1 gene can result in dysregulated substrate cleavage. Alterations in AβPP processing have been of particular interest in research attempting to understand the cause of AD (Selkoe & Hardy 2016). AβPP is a single-pass transmembrane protein that is present in the cell in multiple isoforms: AβPP695, AβPP751 and AβPP770. Each isoform is differentially expressed depending on the tissue. In the brain, AβPP695 is predominately expressed and is crucial to neuronal growth and maturation, especially during development (Coronel et al 2019). Each of the AβPP isoforms are proteolytically cleaved in two distinct pathways which are highly dependent on cellular trafficking of AβPP. Post-translational modifications, such as glycosylation, are known to mediate trafficking through the secretory and endo-lysosomal pathways. N-glycosylated AβPP (Immature AβPP) is held in the

endoplasmic reticulum, whereas the modification of O-glycosylation sites promotes AβPP (mature AβPP) movement to the cell membrane (Hoffmann et al 2000, Wang et al 2017). Mature O-glycosylated AβPP is also more likely to be held in the cell membrane (Chun et al 2015b). This can significantly increase protein interactions which are favourable for non-amyloidogenic AβPP cleavage (*Figure I*).

In fact, a reduction in the ratio between mature and immature AβPP forms has been studied as a biomarker of AD in peripheral tissues (Akingbade et al 2018, Elsworthy & Aldred 2019). Cleavage of AβPP at the cell membrane can be initiated by an α–secretase of which ADAM10 has been identified as the major physiologically relevant enzyme (Kuhn et al 2010). This pathway liberates the neuroprotective secreted AβPP-α (sAβPP-α) N-terminal fragment and an 83-amino acid C-Terminal Fragment (CTF). The cleavage of this CTF by γ-secretase results in the formation of p3 (Chow et al 2010, O'Brien & Wong 2011). Alternatively, immature AβPP or reinternalized AβPP can be cleaved through the amyloidogenic pathway in which AβPP is first cleaved by a β-secretase enzyme, BACE-1, in the trans Golgi network and endosomal pathways (Chun et al 2015a). This releases the soluble N-terminal fragment, sAβPP-β leaving the Amyloid-β (Aβ) -containing C-terminal fragment C99 anchored to the membrane. Subsequent cleavage by γ-secretase, liberates Aβ-peptides and the AβPP intracellular domain.

The generation of Aβ is physiologically normal, however, in fAD a shift towards amyloidogenic AβPP processing can result in an accumulation of longer forms of Aβ peptides (Chen et al 2017). Longer Aβ peptides have been demonstrated to be more hydrophobic than shorter forms and display an elevated propensity to from soluble oligomeric species, which can significantly disrupt cell membranes and thus are highly cytotoxic (Selkoe & Hardy 2016, Zoltowska et al 2016). The accumulation of Aβ is also thought to be critical in the development of late onset AD, however, this may be as a result of reduced Aβ degradation and clearance from the brain as opposed to elevated Aβ generation (Nalivaeva & Turner 2019). The ratio of Aβ peptides of 42 and 40 amino acids is important and has been shown to distinguish between both fAD and late onset AD compared to cognitively healthy individuals.

As mutations to the PSEN1 gene have been shown to alter the carboxypeptidase-like site of γ-secretase it was initially thought that a ‘gain of toxic function’ was a fundamental aspect in the development of fAD (Scheuner et al 1996). Whether this is mostly related to elevated Aβ42 production or through perturbations effecting other γ-secretase substrates

has been an area of debate (Weggen & Beher 2012). However, this may also be due to a 'loss of function' of the γ-secretase complex resulting in a lowering of total Aβ production, with an increase in the Aβ42:40 ratio and thus, Aβ oligomer formation and altered downstream cell signaling (De Strooper 2007, Potter et al 2013, Xia et al 2015). The propensity for generating longer forms of Aβ has been demonstrated in both PSEN1 mutations, L286V and R278I which are known to cause fAD (Arber et al 2020, Sun et al 2017). Individuals carrying these mutations have displayed symptom onset before the age of 50, often accompanied with extra pyramidal symptoms (Frommelt et al 1991, Ryan et al 2016) and for individuals carrying the R278I mutation, speech impairment is particularly present (Godbolt et al 2004). It is important however, to consider that the effects on Aβ42:40 production are not ubiquitously found across all known PSEN1 mutations (Sun et al 2017). Further, there is some evidence that PSEN1 mutations may impact non-amyloidogenic AβPP processing, resulting in the down regulation of sAβPP-α secretion (Ancolio et al 1997). Although the mechanisms driving this association are unknown. What is clear is that some destabilisation the γ-secretase complex is apparent and can lead to altered substrate interaction and eventually, an AD pathology (Arber et al 2020, Kelleher & Shen 2017, Oikawa & Walter 2019).

There has been considerable interest in the derivation of iPSCs carrying PSEN1 mutations to model AD (Li et al 2016a, Li et al 2016b, Pires et al 2016, Poon et al 2016, Tubsuwan et al 2016) and whether these cell models reflect '*in vivo*' phenotype. Neural induction and maturation of these cells into cortical cultures carrying PSEN1 mutations do exhibit pathological features associated with AD during development (Armijo et al 2017, Ochalek et al 2017). Neural progenitor cells (NPC) with a PSEN1 mutation have been reported to differentiate prematurely, have decreased proliferation and increased apoptosis (Yang et al 2017). Prior to differentiation, NPCs carrying a PSEN1 mutation have elevated Aβ42:40 ratio, suggesting this is an early event in familial AD development (Sproul et al 2014). Further, iPSC derived neurons expressing PSEN1 mutations have been found to exhibit dysfunctional endocytosis linked to an accumulation of β-C-terminal fragments. Endosomal function was rescued using BACE-1 inhibitors (Kwart et al 2019). Astrocytes may also play a role in the pathogenesis of AD, not only by a reduced capacity to support surrounding neurons, but also by directly secreting cytotoxic peptides. Astrocytes derived from iPSCs carrying a PSEN1 mutation have shown increased Aβ production and dysregulated calcium homeostasis. In addition, astrocytes may have an altered cytokine profile and increased oxidative stress

markers, which are considered major features underlying the progression of AD (Oksanen et al 2017). Elevated oxidative stress has been implicated in the progression of AD with the brain being particularly susceptible (Oikawa & Walter 2019). This is due to high energy consumption, a high polyunsaturated fatty acid content and relatively low antioxidant buffering capacity. Elevated oxidative stress and altered mitochondrial function are evident prior to the appearance of Aβ and tau pathology in iPSC derived neurons from people with AD (Birnbaum et al 2018). This suggests that oxidative stress may be an early pathological feature of AD. Further to this, evidence of PSEN1 mutations altering mitochondrial function may lead to elevated superoxide generation and may compromise cellular redox status (Sarasija & Norman 2018).

The aim of this study was to examine changes proteins associated with AβPP metabolism by measuring the ratio of mature and immature AβPP, the expression of mature ADAM10 (mADAM10) and Aβ production in iPSC-derived neuron and astrocyte cultures carrying PSEN1 (L286V, R278I) mutations. In addition, markers of protein and lipid oxidation in combination with antioxidant capacity was assessed to give insight to the redox status of the cells.

Materials and Methods

All reagents were purchased from Sigma, Poole, UK unless otherwise stated. Cells and media were routinely tested for Mycoplasma contamination by luminescence assay (Lonza MycoAlert™ PLUS, LT07-703). For information on cell lines used see *Table 1*.

	Ax0018	**Ax0112**	**R278I**
Diagnosis	Healthy Control	Familial AD	Familial AD
Sample type	Dermal Fibroblast	Dermal Fibroblast	Dermal Fibroblast
Donor sex	Male	Female	Male
Age at sampling (yrs)	74	38	60
Age of onset (yrs)	n/a	39	58
Karyotype	Normal	Normal	Normal
Reprogramming method	Episomal Vector	Episomal Vector	Episomal Vector (Okita et al 2011)
Induction method	Monolayer – Axolbio NIM (Shi et al., 2012)	Monolayer – Axolbio NIM (Shi et al., 2012)	Monolayer – NIM (Shi et al., 2012; Arber et al., 2020)
Mutation	None	PSEN1 (L286V)	PSEN1 (R278I)
APOE status	ε2/ ε2	ε3/ ε3	ε2/ ε4

Table 1. - *Information on cell lines used for modelling Alzheimer's disease and healthy control*

Culturing and Neuralisation of iPSC's to Human Neural Precursor Cells (hNPCs)

fAD PSEN1 (R278I) iPSC line was obtained from Dr Selina Wray (UCL, UK). This tissue was provided under the ethical approval of NHS Research Authority NRES Committee London-Central (REC# 08/H0718/54+5).

R278I cells were cultured for expansion of cell numbers and monitored for colony size and changes in morphology before undergoing neural induction. For neural induction, cells were added to Geltrex™ LDEV-Free hESC-qualified Reduced Growth Factor Basement

Membrane Matrix (ThermoFisher Scientific, A1413201) coated wells and incubated (37°C) with Essential-8 media (E8 Media, ThermoFisher Scientific, A15170001) exchange daily until cells reached 100% confluency as a continuous monolayer. At this point, cell media was removed, and Neural induction media (NIM) was added (*see Table 2*). iPSCs were differentiated using Dual SMAD inhibition (Chambers et al 2009, Shi et al 2012). Briefly, a full media exchange with NIM was carried out for a further 9 days. At day 11 cells were passaged using Accutase™ (1mL). Cells were resuspended in Axol™ Neural Maintenance Media (NMM) (Axol Bioscience Cambridge, UK) with 10µM ROCK inhibitor (10µM) and plated into poly-L-ornithine (20µg/mL) and murine laminin from EHS sarcoma (10µg/mL) coated wells. Cells were incubated for 48hr before a full media exchange with NMM, this was performed every other day for 5 days. Cultures formed typical rosette patterning around 12-14 days. At day 17 onwards, cells were passaged 2:1 using Accutase™ and maintained with NMM exchange every other day to allow for spontaneous differentiation and maturation as described below (*section 2.2*).

Table 2. - *Neural induction media (NIM) made by the addition of small molecule signaling pathway inhibitors to Essential 6 as a base medium.*

COMPONENT	AMOUNT
GIBCO™ ESSENTIAL 6™ MEDIUM (THERMOFISHER SCIENTIFIC, A1516401	50mL
XAV939 (STEM CELL TECHNOLOGIES, 72672)	10µL
LDN193189 (STEM CELL TECHNOLOGIES, 72147)	0.5µL
SB431542 (STEM CELL TECHNOLOGIES, 72232)	50µL

Expansion of hNPCs and Preparation of Cell Lysates

Healthy control (AX0018) and PSEN1 mutation L286V (AX0112) hNPCs were purchased from Axol Bioscience (Cambridge, UK).

Control and L286V cells were seeded at a density of $7x10^4$ cells/cm^2 in NMM on poly-L-ornithine (20µg/mL) and murine laminin from EHS sarcoma (10µg/mL) coated wells. Once the cells reached 80% confluency, they were passaged by discarding the spent media from the culture and rinsing with D-PBS. To detach the cells, 1 mL/well Accutase™ was distributed over the cell layer and incubated for 5 minutes at 37°C. 4 mL/well NMM was added to stop the dissociation reaction. Cells were centrifuged at 200 x *g* for 5 minutes. The pellet was resuspended in NMM and cells plated at the same density as above. Cells were incubated in a 37°C, 5% CO_2/ 95% air atmosphere and total media exchanged every other day. Each replicate (n) was expanded through 2 passages, for final plating at passage 3.

hNPC's from Control, L286V and R278I lines were seeded for final plating on poly-L-ornithine (20µg/mL) and laminin (10µg/mL) coated plates. Control, L286V and R278I cells were cultured for a further 45 days to achieve maturation. For the preparation of cell lysates, cell media was removed, and cells were washed with D-PBS without magnesium or calcium. Ice-cold lysis buffer (200 mM NaCl, 10 mM EDTA, 10 mM Na_2HPO_4, 0.5% NP40, 0.1% SDS, 1x protease inhibitors and 5µM GI254023X) was added to cells and incubated for 30 minutes at room temperature. Cells were dissociated from the plate, centrifuged at 10,000xg and the resulting solubilised cell lysate was frozen at -80°C until further use.

Immunocytochemistry

For immunocytochemistry (ICC) experiments were seeded at a density of $2x10^5$ cells/glass coverslip and incubated as described above. Cells were fed with NMM will a full media exchange every other day. Cells to undergo ICC were washed with respective media and fixed in an equal volume of 4% (v/v) paraformaldehyde (PFA) in PBS for 5 minutes. The solution was removed, and cells were fixed again in 4% PFA in PBS for 5 minutes. The cells were washed twice in PBS and incubated for 3 minutes in PBS with 0.2% (v/v) Triton X-100, then again for 5 minutes. To reduce nonspecific binding of antibodies, cells were blocked for 1 hour in PBS containing 0.2% (v/v) Triton X-100 and 2% (w/v) bovine serum albumin.

To identify markers associated with neural induction, cells were incubated Pax6 (901301, BioLegend) and Sox2 (MAB2018, R&D systems) antibodies to detect early neuronal progenitors. Cell cultures were stained for S100β (00095194, Dako), TUJ-1 (Ab7751, Abcam), ADAM 10 (Abcam, AB1997), AβPP (Merck, Mab348), MAP-2 (MA5-12826, Invitrogen),

Synaptophysin (MA5-14532, Invitrogen) and VGLUT1 (135303, Synaptic Systems), after 45 days to assess cellular maturity. Following primary antibody incubation, appropriate secondary antibodies, Alexa Fluor® 488 AffiniPure Goat Anti-Rabbit IgG (1:2000, 111-545-144, Jackson Laboratories) and Alexa Fluor® 633 Goat anti-Mouse IgG (1:2000, A-21052, ThermoFisher Scientific) were co stained. Cells were mounted in a Prolong™ Gold Antifade Mountant with DAPI (P3935, ThermoFisher Scientific) to glass slides and imaged using a Nikon A1R laser scanning confocal microscope (Nikon EU, Netherlands).

Total Cellular Protein Quantification

Protein concentration of cell lysates was determined using a modified protocol of the Bicinchoninic acid (BCA) protein assay (Smith et al 1985) to enable standardisation of assays. Briefly, lyophilised Bovine serum albumin was dissolved in dH_2O to give a final concentration of 1mg/ml. Cell lysates and media were diluted (0.2 – 1.0mg/ml) in lysis buffer (see above). Next, standards were prepared by diluting BSA with dH_2O ranging from 0 – 1mg/ml. Sample or standard (10µL) was added to the appropriate well/s in triplicate and covered until later use. Copper sulphate was mixed with BCA in a 51:1 ratio to obtain the necessary volume and added to each well (200µL). The plate was then incubated at 37°C for 30 minutes and protected from light. The absorbance of the plate was then read at 540nm.

SDS-PAGE and Western Blotting

The protocol used for SDS-PAGE and western blotting were adapted from Manzine et al. (2013) with minor modifications. Cell lysate (20µg) was heated for 5mins at 95°C and loaded in duplicate into 8% SDS- PAGE gels. Molecular weight markers were used to check molecular weight and protein transfer (Amersham ECL Rainbow marker, RPN800E). After electrophoresis, the proteins were transferred to nitrocellulose membranes (Amersham protran 0.2µm) using the Mini Trans-Blot Cell transfer system (BioRad) for 1 hour. Ponceau S Solution was added to membranes to visualise total protein transfer and check even sample loading. Membranes were blocked with 5% milk in TBST 0.1% for 1 hour and washed in 0.1% TBST. Membranes were then incubated with anti-ADAM 10 (Abcam, AB1997), AβPP (Merck, Mab348) followed by incubation with corresponding secondary antibodies (Abcam Anti-rabbit HRP-linked H&L IgG AB6721, Sigma Anti-mouse IgG FC-specific A0168). The membranes were developed using ECL substrate (Clarity Western, Biorad) according to

manufacturer instruction and imaged using C-digit scanner (Licor). Finally, bands were quantified using Image Studio (Licor).

Quantification of Amyloid-β Peptides 1-40 And 1-42

To determine the amount of Aβ 1-40 and 1-42 in spent media, enzyme-linked immune absorbent assays were carried out according to manufacturer's instruction (ThermoFisher, KHB3481, KHB3441). A serial dilution of standards was prepared using synthetic Aβ peptide (0pg/ml – 500pg/mL) and this was added to appropriate wells (50µL). Samples (collected cell media) were also added to appropriate wells (50µL) in duplicate and the *Hu biotinylated Aβ 1-40 or 1-42 detection antibody* (50µL) was then added to samples and standards and incubated for 3 hours at room temperature. Each well was then washed four times with wash buffer (1x, 300µL). Anti-rabbit IgG HRP was added to each well (100µL) and incubated for 30 minutes in the dark at room temperature. Wells were washed as previously described and stabilised chromogen was added (100µL) followed by a further 30-minute incubation in the dark at room temperature. Finally, stop solution was added to each well (100µL) and the absorbance was read at 450nm.

Quantification of Oligomeric Amyloid-β

To determine the amount of oligomeric Aβ in spent media, an enzyme-linked immune absorbent assay was carried out according to manufacturer's instruction (ThermoFisher, KHB3491). A serial dilution of standards was prepared using synthetic aggregated Aβ (0ng/ml – 5.7ng/ml) and this was added to appropriate wells (100µL). Samples (collected cell media) were also added to appropriate wells (100µL) in duplicate and incubated for 2 hours at room temperature. Each well was then washed four times with wash buffer (1x, 300µL). *Hu aggregated Aβ biotin conjugate* (100µL) was added to each well and incubated for 1 hour. A further wash step was carried out, then Streptavidin-HRP working solution (100µL) was added and incubated for 30 minutes. Wells were washed as previously described and stabilised chromogen was added (100µL) with a further 30-minute incubation in the dark at room temperature. Finally, stop solution was added to each well (100µL) and the absorbance was read at 450nm.

Quantification of sAβPP-α

To quantify s*A*βPP-α, cell media was collected after 48hrs from the cultures and analysed by Sandwich ELISA (MyBioSource, MBS9358454). Briefly, a serial dilution of pre-prepared standards were added (0ng/mL – 100ng/mL) to appropriate wells (50µL). Samples (collected cell media) were also added to appropriate wells (50µL) in duplicate and incubated for 1 hour at 37°C with HRP-conjugate reagent (100µL). Each well was then washed four times with wash buffer (1x, 300µL). Chromogen solution A (50µL) and B (50µL) were added to each well followed by incubation for 15 minutes at 37°C protected from light. Finally, stop solution was added to each well (50µL) and the absorbance was read at 450nm.

Protein Carbonyl Formation

Protein Carbonylation was assessed by the method of Carty et al. (2000). Briefly, cell lysates and standards (BSA) were added to carbonate buffer (sodium carbonate 50mM, pH 9.2) and plated into 96 well plates (50µl at 0.05mg/ml) in triplicate. Protein was allowed to bind for 1h at 37°C before washing with TBS–Tween (0.5%). DNPH was added in 2M HCl (1mM) and allowed to react for 1h at room temperature before washing as before. Non-specific binding sites were blocked overnight at 4°C with TBS-tween (1%). After washing, rabbit anti-DNPH primary antibody (1:1000) was applied and incubated for 1h at 37°C and, following washing with TBS/Tween, anti-rabbit IgE conjugated to peroxidase (1:5000) was also incubated at 37°C for 1h. The reaction was visualised by o-phenylenediamine tablets with hydrogen peroxide (8µl) in citrate-phosphate buffer (10mL) and stopped by addition of sulphuric acid (2N). Absorbance was read at 490nm.

Total F2 8-Isoprostanes

Total 8-isoprostanes were measured using a commercially available ELISA kit to assess lipid peroxidation (8-isoprostane ELISA kit, Cayman Chemical). Prior to this assay the cell lysate samples were purified following the manufacturer's instructions. Briefly, cell lysate was added to the 8-isoprostane affinity sorbent (401113, Cayman Chemical) and incubated for 60 minutes with gentle mixing. Samples were then centrifuged at 1500xg for 30 seconds to sediment the sorbent, the resulting supernatant was removed and discarded, this was repeated 2 times following the addition Eicosanoid Column Affinity buffer (100µL, 400220, Cayman Chemical) and ultrapure water (100µL). Elution solution (95% ethanol) was then added to the sediment and evaporated to dryness under nitrogen. Samples were suspended

in the ELISA buffer. Standards were then prepared from the assay stock solution to create an 8-point standard curve ranging from 0.8 to 500pg/mL, ELISA buffer was used as the 0pg.mL standard. Standard or lysates (50µL) were added to the appropriate well with 8-isoprostane tracer (50µL) and antiserum (50µL) in triplicate, this was incubated for 18hours at 4°C. Ellman's reagent was added to each well (200µL) and left to incubate for 2 hours with gentle agitation. The plate was then read at 420nm.

Total Antioxidant Capacity

Cell lysates were diluted 1:1 with ultrapure water (Millipore). Standards were freshly prepared using Ascorbic acid to create a 7-point standard curve ranging from 0µM to 1000µM. Sample or standard (10µL) was then pipetted into wells a 96-well microtiter plate in duplicate. The working reagent was made by combining acetate buffer (30ml, 300mM), TPTZ solution (3mL, 10.6mM) and ferric chloride solution (3ml, 20mM) before being added to each well (300µL). The plate was then incubated for 8 minutes at room temperature. Plate reading was completed at 650nm and values were calculated using linear regression. Values were expressed as µM of antioxidant power relative to ascorbic acid corrected for total cellular protein content.

Statistical analysis

To generate standard curves from plate-based assays either linear regression or 4-paramaeter logistic regression was used to plot known concentrations against optical absorbance at specified wavelengths according to manufacturer's instruction. From this sample concentrations were calculated and normalized to total protein concentration in corresponding cell lysate. All quantitative data in the text and figures are presented as Mean ± S.D. unless otherwise stated. Significance was calculated using ordinary one-way ANOVA with Bonferroni *post hoc* corrections and using linear regression models. All data was processed using GraphPad Prism (Version 8.4.3).

Results

Cell Characterisation

To monitor cell morphology and similar development between cell lines images from brightfield microscopy were captured routinely (EVOS XL core, Thermo Fisher Scientific). Images of iPSCs, early NPCs and cultures at 45days can been seen in *Figure 1*.

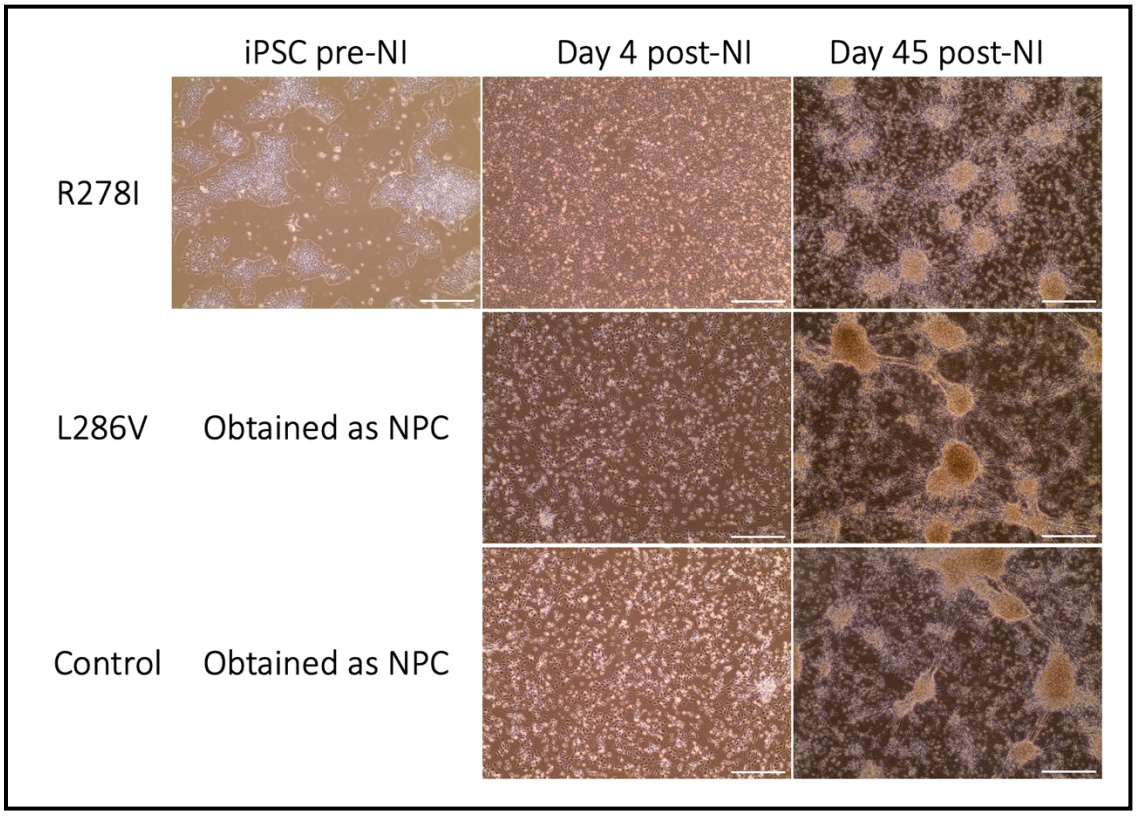

Figure 1 – *Representative brightfield microscopy images of cultured cells. PSEN1 mutation, R278I, shown in top left box as iPSC colonies pre neural induction (NI). Representative images of Neural precursor cells at day 4 post NI can bee seen in column two. Neural rosette patterning, followed by maturation and organization into 'hub-like' patterns were seen in each cell line at day 45 post final plating of NPCs (Scale bars to 100µm).*

ICC staining was utilised to characterise neuralisation of cells. After 7 days in culture neuritic protrusion becomes apparent with the formation of rosette patterning, which is indicative of a neuronal fate (Shi et al 2012). hNPCs, although directed towards a cortical lineage suggested by the Pax6 staining, also maintain a pluripotent state with the potential to form a range of cortical cells shown by positive SOX2 staining (*Figure 2.1.*). Initially,

spontaneous differentiation of NPCs leads to the development of more mature neuronal cell types. With continual maturation, NPC cultures began to develop glial cells which surround neurons and supply nutrients, supporting neuronal growth (Crompton et al 2017). These cells are key progenitor cells undergoing neurogenesis or gliogenesis whereby astrocytes are developed. After 45 days of culture, distinct neuronal and glial cells can be seen by TUJ-1 and greater S100β expression respectively (*Figure 2.2)*. Neurons form more hub-based characteristics with longer axonal processes which are positive for the pre-synaptic protein synaptophysin (*Figure 2.3)*. Cell cultures were also positive for ADAM10, AβPP (*Figure 2.4)* and for the expression of vGLUT1 excitatory neurons (*Figure 2.5*).

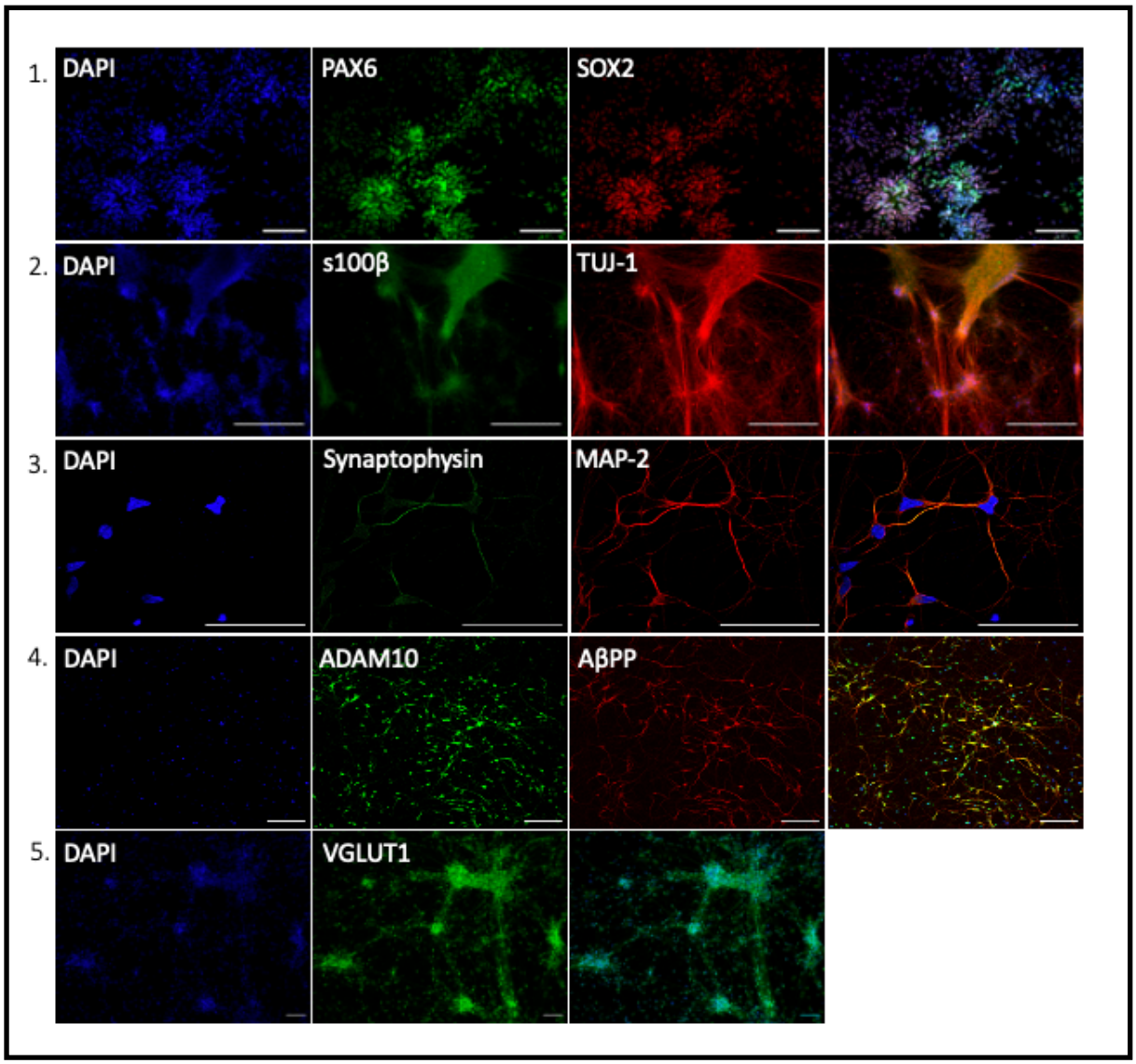

Figure 2 – *Representative confocal microscopy images of cultured cells with ICC staining.* ***Row 1****: Healthy control NPCs (day 7 post differentiation) were fixed and stained using DAPI nuclear stain (Blue), Pax6 (green) and Sox2 (red) showing neural rosette patterning (Scale bars to 100µm).* ***Row 2:*** *Neurons and astrocytes (Healthy control, day 45). DAPI nuclear stain (Blue), s100β (green), TUJ1 (red) (Scale bars to 200µm).* ***Row 3****: Mature neuronal staining with synaptic proteins (L286V, day 40) with ICC staining for DAPI (blue), synaptophysin (green) and Map2 (red) (Scale bars to 50µm).* ***Row 4****: Neuron/astrocyte cultures showing expression of DAPI (blue), ADAM10 (green) and AβPP (red) (Scale bars to 100µm).* ***Row 5****: ICC staining of deep layer excitatory neurons (Healthy control, day 45). DAPI nuclear stain (Blue) and VGLUT1 (green) (Scale bars to 50µm).*

ADAM10 expression, AβPP ratio and Aβ are Altered in PSEN1 Mutations

The mature, enzymatically active ADAM10 protein (mADAM10, AU) was significantly lowered in L286V (0.081 ± 0.016, p = 0.008) cells compared to healthy control (0.117 ± 0.016). Cells carrying the PSEN1 mutation R278I (0.0465 ± 0.007, p = 0.022) showed a further

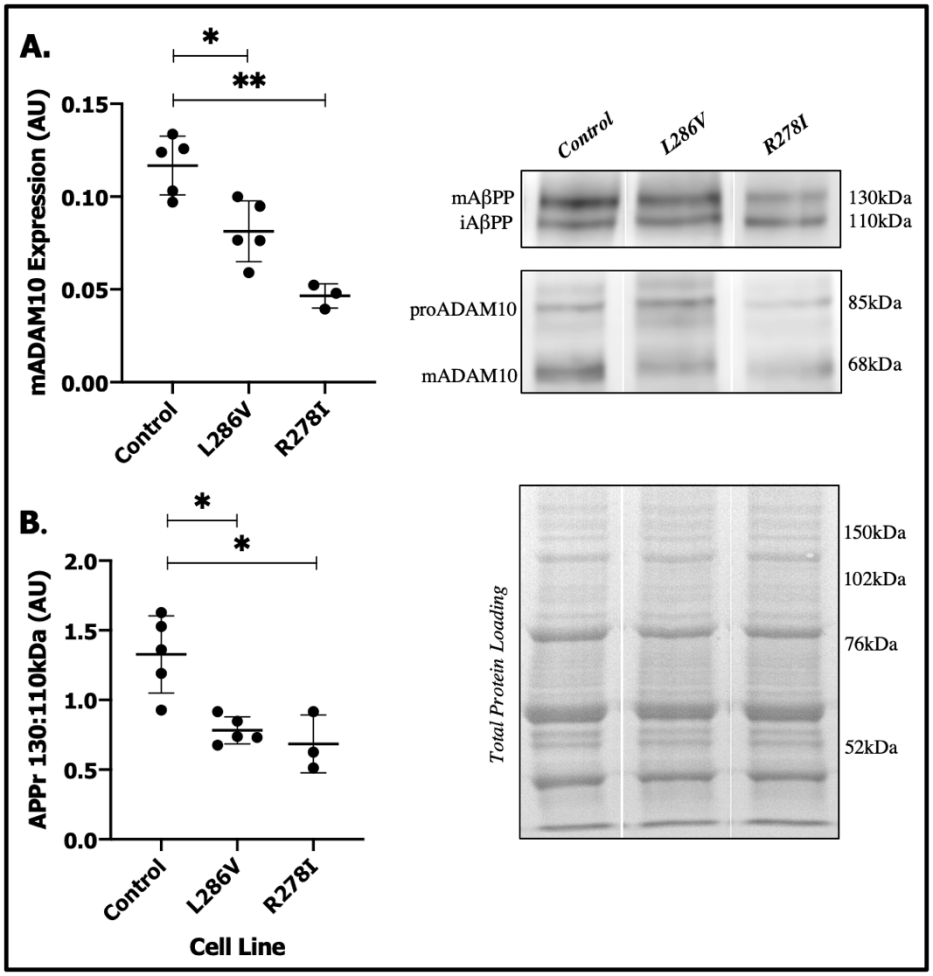

reduction in mADAM10 expression compared to L286V (*Figure 3, **A**.).* In addition, the AβPP ratio (AU) was significantly altered with PSEN1 mutations. Both L286V (0.782 ± 0.098, *p* = 0.024) and R278I (0.685 ± 0.208, *p* = 0.021) cells had a significantly lower AβPP ratio than control (1.327 ± 0.278). There was no significant difference between PSEN1 mutations (*p* > 0.050) (*Figure 3, **B**.*).

Figure 3 - *Graphs showing the individual data points for cell lysates (45 days old) analysed via western blotting relative to total protein densitometry. Cell lysates from healthy control (n=5), L286V (n=5) and* R278I *(n=3) were separated using SDS-PAGE electrophoresis followed by western blotting. Densitometry was quantified using Licor C-digit and image studio software.* ***A.*** *mADAM10 expression (AU) normalised to total protein densitometry which can be seen on the right. Representative blot images show both the immature 85kDa proADAM10 and mature/active 68kDa mADAM10 detected by Ab1997 antibody corresponding to table above.* ***B.*** *AβPP ratio quantified by the ratio of bands at 130kDa to 110kDa. Representative blotting images of AβPP bands detected using Mab348 antibody corresponding to table above.*

**Significantly different to matched Cell Line (p<0.05) **(p<0.01)*

To determine the amount of amyloidogenic AβPP processing, Aβ peptides 1-40 and Aβ1-42 (pg/mL) were quantified in conditioned cell media. Both Aβ1-40 and Aβ1-42 were significantly elevated in L286V (319.10 ± 59.98, *p* = 0.003 & 191.70 ± 36.17, *p* = 0.016) and R278I cells (300.00 ± 53.28, *p* = 0.016 & 370.40 ± 10.79, *p* = 0.001) compared to healthy control (174.3 ± 35.30 & 130.90 ± 23.82) (*Figure 4 **A** & **B.***). The combined Aβ1-40 and Aβ1-42 production was significantly increased in L286V (520.80 ± 84.72, *p* = 0.008) and R278I (670.40 ± 57.11, *p* = 0.001) cells compared to healthy control (305.20 ± 17.74) (*Figure 4 **C.***). The ratio of Aβ1-42:40 was only significantly higher in R278I (1.263 ± 0.2423, *p* = 0.022) cells compared to healthy control (0.7895 ± 0.2440) (*Figure 4 **D**.*). Further, Aβ oligomers (ng/mL) were significantly elevated in R278I cells (0.8680 ± 0.1077) compared to control (0.4369 ± 0.0361, *p* = 0.001) and L286V cells (0.4712 ± 0.0408, *p* = 0.001) (*Figure 4 **E***). Finally, sAβPP-α (ng/mg/mL) in conditioned cell media was significantly lower in L286V (3.120 ± 0.4110, *p* = 0.0162) compared to healthy control (4.516 ± 0.537). sAβPP-α was not significantly altered in R278I (3.714 ± 0.287, *p* > 0.05) (*Figure 4 **F.***).

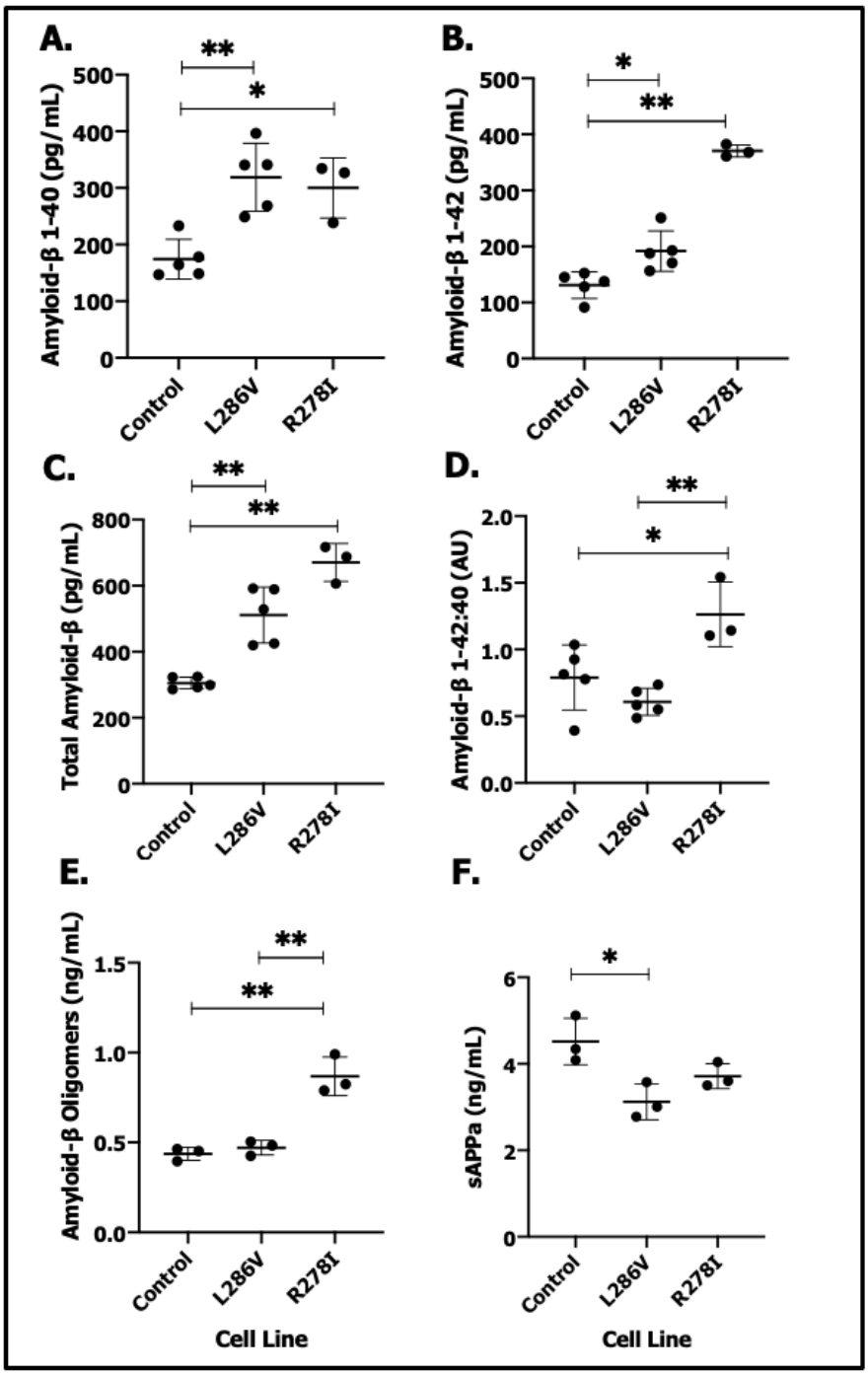

Figure 4 - *Graphs showing the individual data points for media concentration of* **A.** *Aβ1:40 and* ***B.*** *Aβ1-42 (pg/mL) analysed via ELISA in Healthy control (n=5), L268V (n=5) and* R278I *(n=3) at day 45.* C. *Shows the sum of Aβ1:40+1:42 peptides to give total amyloid Aβ1:40 and 1:42 secretion.* D. *The ratio of Aβ1:42 to Aβ1:40 is shown in Arbitrary units (AU).* E. *Aβ oligomers (ng/ml)* F. *sAβpp-a (ng/mL). n=3 for each cell line.*

**Significantly different to matched Cell Line (p<0.05) **(p<0.01)*

Redox Balance is Perturbed in Co-Cultures Carrying PSEN1 Mutations

To quantify cellular redox balance, markers of oxidative stress and cellular antioxidant capacity were measured. Protein carbonylation (mg/mL) was significantly elevated in both L286V (27.87 ± 8.800, $p = 0.004$) and R278I (39.10 ± 4.088, $p = 0.001$) cells compared to control (13.06 ± 5.365) (*Figure 5,* ***A***.). In addition, total 8-isoprostanes (pg/mL) was elevated in L286V (3.867 ± 0.7670) cells compared to both control (1.210 ± 0.6283, $p = 0.001$) and R278I (2.477 ± 0.1964, $p = 0.034$) cells (*Figure 5,* ***B***.). Cellular antioxidant capacity (µM/mg) was significantly lowered in R278I (48.37 ± 7.447) cells compared to control (141.3 ± 38.22, $p = 0.003$) and L286V (135.1 ± 34.18, $p = 0.005$) cells (*Figure 5,* ***C***.).

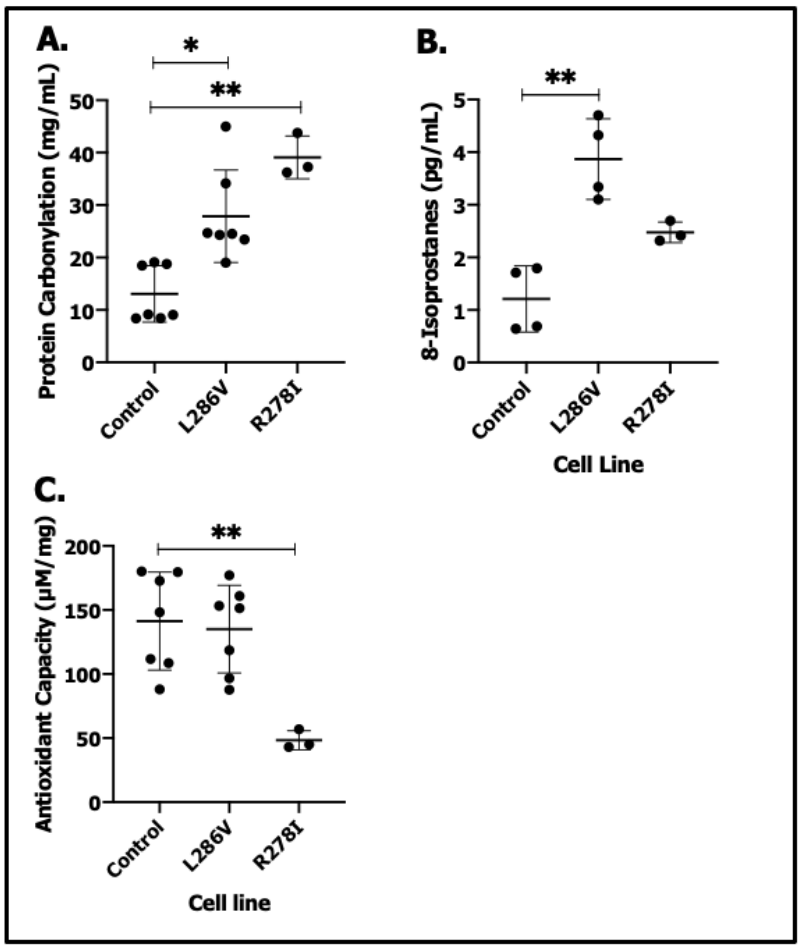

Figure 5 - *Graphs showing the individual data points for markers of redox balance in cell lysates normalised to cellular protein content.* ***A.*** *Protein carbonylation in healthy control (n=7), L286V (n=7) and R278I (n=3) measured via ELISA* (mg/mL) *B. Total 8-isoprostanes in immunopurified lysate preparations from healthy control (n=4), L286V (n=4) and R278I (n=3) quantified by ELISA* (pg/mL) ***C.*** *Cellular antioxidant capacity relative to ascorbic acid*

measured in healthy control (n=7), L286V (n=7) and R278I (n=3) using colorimetric assay (µM/mg).

**Significantly different to matched Cell Line (p<0.05) **(p<0.01)*

Further analysis across all cell lines showed higher amounts of protein carbonylation was significantly associated with lower mADAM10 expression ((F(1,11)=19.020, *P = 0.001)* R^2 *= 0.634)* and with AβPP ratio ((F(1,11)=10.670, *P = 0.001)* R^2 *= 0.492)* (*Figure 6, **A** & **B**.*).

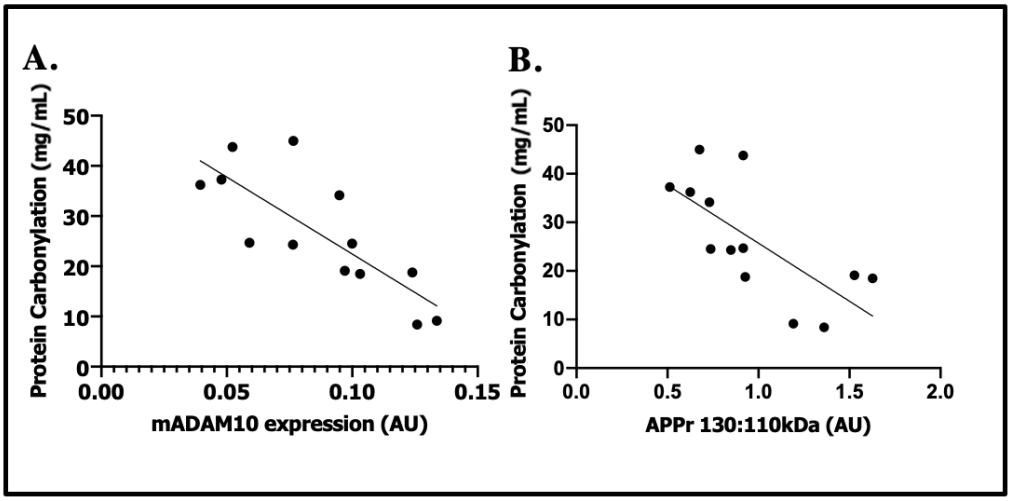

Figure 6 – *Regression analysis between markers of oxidative stress and AβPP processing. **A.** Protein carbonylation (mg/mL) and mADAM10 expression (AU) measured via ELISA and Western blot respectively. **B.** Protein carbonylation (mg/mL) and AβPP ratio (AU) measured via ELISA and Western blot respectively.*

Discussion

The continued development of iPSC technology has the potential to enable detailed investigation into disease pathology and drug screening. However, for this to be possible it is essential that iPSC-derived models display a phenotype similar to that seen '*in vivo*'. A crucial step in this process is to characterise and closely monitor cellular development to achieve the desired cell fate. Data presented herein demonstrated that proteins involved in AβPP processing were significantly altered in PSEN1 co-cultures. PSEN1 co-cultures also had altered redox status compared to control co-cultures. These features are important characteristics of AD and therefore, this '*in vitro*' model represents a functional system to study the early pathological features of AD.

After differentiation of iPSC's into co-cultures of neurons and astrocytes, markers indicative of altered AβPP processing were quantified. Interestingly, both PSEN1 mutations showed a reduction in mADAM10 protein expression, matched by a lower AβPP ratio in both PSEN1 mutations. A reduction in the AβPP ratio is supported by several studies investigating potential biomarkers of AD in both central and peripheral tissues (Akingbade et al 2018). An altered AβPP ratio may be indicative of a reduced amount of AβPP reaching the cell membrane. This may be due to the changes in the glycosylation of the protein and may therefore result in a reduced interaction of mature AβPP with mADAM10 (Akasaka-Manya et al 2017, Wang et al 2017). Interestingly, the product from cleavage of AβPP by mADAM10, sAβPPα, appeared lower in both PSEN1 mutations. However, this only reached significance in the L268V mutation. Although ADAM10 cleavage is not exclusive to sAβPPα, this is indicative of a lower ADAM10 activity when combined with both measures of mADAM10 and AβPP ratio protein levels.

The nature of PSEN1 mutations directly impacts the function of the catalytic subunit of the γ-secretase enzyme. However, whether such mutations lead to a gain of toxic function or a loss of normal γ-secretase function is still under debate (De Strooper 2007, Kelleher & Shen 2017). Interestingly, the two PSEN1 mutations characterised herein highlight this problem. In PSEN1 L286V cells, total Aβ was significantly higher than the PSEN1 R278I mutation. Although total Aβ was also elevated in R278I cells this was not statistically significant compared to health control cells. Yet, the ratio of Aβ1-42:40 was shifted towards Aβ1-42 generation in the PSEN1 mutation R278I, which was more different to controls than L286V cells, where the ratio of Aβ1-42:40 was unchanged compared to control. Interestingly,

previous research has also shown the PSEN1 mutation R278I, has a significantly higher Aβ1-42:40 ratio compared to other fAD mutations (Arber et al 2020). This shift is indicative of an altered AβPP cleavage site preference by γ-secretase. Aβ1-42:40 ratio is often used as a Cerebral Spinal Fluid marker to aid diagnosis of AD (Hansson et al 2019, Pannee et al 2016). An increase in longer forms of Aβ is associated with a greater propensity for aggregation. This was supported by the finding of increased Aβ oligomers in R278I cells, which had the most elevated Aβ1-42. Thus, there is understandably growing attention around the hypothesis that different PSEN1 mutations can lead to varied Aβ production (Arber et al 2020, Kwart et al 2019, Woodruff et al 2013).

Oxidative stress is common feature of neurodegenerative diseases, metabolic disorders and even healthy ageing (Butterfield & Halliwell 2019). However, understanding the cellular redox balance of specific cell populations may be critical to understanding pathological processes. Neurons are particularly susceptible to oxidative stress due to their high energy demand, with astrocytes playing a key role in neuroprotection by supporting cell metabolism (Allen & Eroglu 2017, Butterfield 2018). Therefore, neuron and astrocyte co-cultures can replicate a closer model to monitor '*in vivo*' cell stress. Both PSEN1 mutations used in the study herein displayed elevated protein oxidation markers and this was significantly associated with a reduction in both mADAM10 and mature AβPP relative to immature AβPP. This link may be explained by the addition of protein carbonyl groups directly effecting normal protein function or trafficking, which is crucial for the maturation of both ADAM10 and AβPP. This highlights an interesting direction for future research. Elevated oxidative stress could be further seen in R278I cells, which had a significantly lowered antioxidant capacity, however, lipid oxidation was only significantly elevated in L286V cell compared to both R278I and 'healthy' control cells.

The insertion and interaction of Aβ1-42 with lipid membranes has been linked to reactive oxygen species (ROS) propagation of oxidised lipids and proteins (Butterfield & Halliwell 2019). The tendency of cells carrying the PSEN1 mutation to generate longer Aβ peptides relative to shorter forms of Aβ can increase the likelihood of oligomerisation. This may in part explain the association of PSEN1 mutations with elevated oxidative damage markers. However, Aβ oligomers were unchanged in L286V cells suggesting an oxidative stress may occur independently from Aβ oligomer formation. As F8-isoprostanes was the only marker of lipid peroxidation measured it may be possible that other modified lipids are

more closely linked to Aβ oligomers such as, 4-hydroxynonenal adducts (Butterfield 2020). Further, it should be noted that this study only focuses on Aβ1-42/40, whereas Aβ exists in a number of deferent C- and N- terminally truncated forms (Arber et al 2020). More data on a larger number of Aβ peptides of varying length in PSEN1 mutations is warranted to further investigate the link between Aβ-cell membrane interaction and lipid oxidation.

The utlisation of cultures co-expressing both neurons and astrocytes is an important step in producing better models of AD. Astrocytes play a key role in supporting in maintaining neuronal function, substrate transport/ metabolism and neuroprotection (Rodríguez-Arellano et al 2016). This research shows that such co-cultures carrying a PSEN1 mutation display perturbed features associated with AβPP processing and redox balance. However, using a spontaneous differentiation protocol, it is incredibly difficult to distinguish the contribution of each cell type to the observed phenotype. Equally, the proportion of mature astrocytes relative to the mature human brain present at 45 days after final plating (~65 day post differentiation) is likely low. This highlights an interesting avenue for future research comparing both mono-cultures and synchronised co-cultures of neurons and astrocytes, whereby better control over physiological neuron/astrocyte ratios can be modelled to investigate the role of each cell type in disease. Further to this, it is important to acknowledge the relative immaturity of the cells using this method of culture. Whilst markers of mature neurons and astrocytes are present and display functional signaling attributes (Shi et al 2012), there is likely still a proportion of neural precursor cells representing an early neurodevelopmental stage. Whether the fAD mutations effect the process of neurogenesis was not investigated in this study. However, recent evidence of premature neurogenesis in iPSC-derived neurons carrying PSEN1 mutations has been found (Arber et al 2021). This may represent a 'premature brain ageing' phenotype in people with fAD and should be further investigate in iPSC-derived cell models. Despite this, the generation of iPSC-derived cell models has been hugely successful for identifying early pathological features of monogenic diseases, such as PSEN1 fAD mutations. Although not used in this research, the use of isogenic cell lines has been used to strengthen conclusions from iPSC cell models by controlling for confounding genetic variance within patient samples (Arber et al 2019).

The number of patient samples and biological repeats, although reasonable for this line of research, are low for statistical analysis. By itself, this reduces the generalisability of the outcomes found on how PSEN1 mutations effect cortical cell types, however, the

contribution of this work to the rapidly growing area of iPSC research should not be understated. In fact, the accumulating evidence supports the utility of iPSC-derived cortical cell types for investigating early disease mechanisms and may be useful for screening therapeutic treatments in the near future.

Taken together, the findings highlight the need for more research into how PSEN1 mutations may result in perturbed ROS production and leading towards oxidative stress cascades. The research methods applied are not limited to AD related mutations. Applying the methods used to examine oxidative stress into iPSC-derived neurons from individuals with Parkinson's disease may be of particular interest. Defective mitochondria, axonal transport and mitophagy have been identified in Parkinson's Disease patient iPSC-derived neurons and may be linked to redox imbalance in early neurodevelopmental stages (Trombetta-Lima et al 2021).

Conclusion

In conclusion, this study provides evidence that PSEN1 mutations in iPSC-derived neuron and astrocyte co-cultures can lead to significant alterations in AβPP processing accompanied by a change in the redox status of the cell. These changes are present in the pathology of AD. A reduction in both the AβPP ratio and mature ADAM10 protein levels, in combination with altered generation of sAβPPα, Aβ1-40 and Aβ1-42 was found in cells carrying PSEN1 mutations compared to 'healthy' control. Notably, levels of Aβ in monomeric and oligomeric forms also varied between PSEN1 mutations. In addition, elevated oxidative stress was apparent in cells with a PSEN1 mutation compared to control. This study provides data to suggest that iPSC-derived cell networks are a valuable tool to investigate genetic mutations associated with AD, however it is crucial consider the differential effects individual PSEN1 mutations may have on different cell types during the progression of the AD. Future studies will help to better understand the causative mechanisms associated with PSEN1 mutations and fAD which in turn, will facilitate the development of therapeutic inventions.

Acknowledgments

The authors would like to thank Dr Selina Wray (University College London, UK) for kindly providing the fAD PSEN1 (R278I) iPSC line.

Funding

This work was supported by Alzheimer's Research UK [ARUK-NC2018-MID].

Conflict of Interest

The authors declare that the research was conducted in the absence of any commercial or financial relationships that could be construed as a potential conflict of interest.

Author Contributions

RJE[1] contributed to this manuscript as primary author. This included co-authoring grant application, developing research questions, culturing and analysis of the cells and initial drafting of the text.
AG[2] was involved in the development of the cell culture protocol and was also involved in the ICC imaging.
EF[1] played a significant role in the data collection methods and provided a review in the initial write up of the manuscript.
AL[2] was responsible for the iPSC expansion and maintenance of iPSC cells and provided a review of the manuscript drafting.
JC[2] was involved in the development of the cell culture protocol and contributed to the background write up of the manuscript.
MK[2] was responsible for the neural induction and expansion of cells and provided a review of the manuscript drafting.
SA[2] collected conditioned cell media and analysed Amyloid-beta peptides species and immunofluorescence imaging.
EJH[2] is the co-author of the grant application funding this research and was the leading expert in designing the cell methods. EJH also provided a final review of the manuscript.
SA[1, 3] is the PI of RJE and was the lead application of the grant application funding this research. SA is also responsible for advising on the oxidative stress measures and ADAM10 measurements. SA also provided a final review of the article.

References

Akasaka-Manya K, Kawamura M, Tsumoto H, Saito Y, Tachida Y, et al. 2017. Excess APP O-glycosylation by GalNAc-T6 decreases Aβ production. *J Biochem* 161: 99-111

Akingbade OES, Gibson C, Kalaria RN, Mukaetova-Ladinska EB. 2018. Platelets: Peripheral Biomarkers of Dementia? *J Alzheimers Dis* 63: 1235-59

Allen NJ, Eroglu C. 2017. Cell Biology of Astrocyte-Synapse Interactions. *Neuron* 96: 697-708

Ancolio K, Marambaud P, Dauch P, Checler F. 1997. Alpha-secretase-derived product of beta-amyloid precursor protein is decreased by presenilin 1 mutations linked to familial Alzheimer's disease. *J Neurochem* 69: 2494-9

Arber C, Lovejoy C, Harris L, Willumsen N, Alatza A, et al. 2021. Familial Alzheimer's Disease Mutations in PSEN1 Lead to Premature Human Stem Cell Neurogenesis. *Cell Rep* 34: 108615

Arber C, Toombs J, Lovejoy C, Ryan NS, Paterson RW, et al. 2020. Familial Alzheimer's disease patient-derived neurons reveal distinct mutation-specific effects on amyloid beta. *Mol Psychiatry* 25: 2919-31

Arber C, Villegas-Llerena C, Toombs J, Pocock JM, Ryan NS, et al. 2019. Amyloid precursor protein processing in human neurons with an allelic series of the. *Brain Commun* 1: fcz024

Armijo E, Gonzalez C, Shahnawaz M, Flores A, Davis B, Soto C. 2017. Increased susceptibility to Aβ toxicity in neuronal cultures derived from familial Alzheimer's disease (PSEN1-A246E) induced pluripotent stem cells. *Neurosci Lett* 639: 74-81

Birnbaum JH, Wanner D, Gietl AF, Saake A, Kündig TM, et al. 2018. Oxidative stress and altered mitochondrial protein expression in the absence of amyloid-β and tau pathology in iPSC-derived neurons from sporadic Alzheimer's disease patients. *Stem Cell Res* 27: 121-30

Butterfield DA. 2018. Perspectives on Oxidative Stress in Alzheimer's Disease and Predictions of Future Research Emphases. *J Alzheimers Dis* 64: S469-S79

Butterfield DA. 2020. BRAIN LIPID PEROXIDATION AND ALZHEIMER DISEASE: SYNERGY BETWEEN THE BUTTERFIELD AND MATTSON LABORATORIES. *Ageing Res Rev*: 101049

Butterfield DA, Halliwell B. 2019. Oxidative stress, dysfunctional glucose metabolism and Alzheimer disease. *Nat Rev Neurosci* 20: 148-60

Chambers SM, Fasano CA, Papapetrou EP, Tomishima M, Sadelain M, Studer L. 2009. Highly efficient neural conversion of human ES and iPS cells by dual inhibition of SMAD signaling. *Nat Biotechnol* 27: 275-80

Chen GF, Xu TH, Yan Y, Zhou YR, Jiang Y, et al. 2017. Amyloid beta: structure, biology and structure-based therapeutic development. *Acta Pharmacol Sin* 38: 1205-35

Chow VW, Mattson MP, Wong PC, Gleichmann M. 2010. An overview of APP processing enzymes and products. *Neuromolecular Med* 12: 1-12

Chun YS, Kwon OH, Oh HG, Kim TW, McIntire LB, et al. 2015a. Threonine 576 residue of amyloid-β precursor protein regulates its trafficking and processing. *Biochem Biophys Res Commun* 467: 955-60

Chun YS, Park Y, Oh HG, Kim TW, Yang HO, et al. 2015b. O-GlcNAcylation promotes non-amyloidogenic processing of amyloid-β protein precursor via inhibition of endocytosis from the plasma membrane. *J Alzheimers Dis* 44: 261-75

Coronel R, Lachgar M, Bernabeu-Zornoza A, Palmer C, Domínguez-Alvaro M, et al. 2019. Neuronal and Glial Differentiation of Human Neural Stem Cells Is Regulated by Amyloid Precursor Protein (APP) Levels. *Mol Neurobiol* 56: 1248-61

Crompton LA, Cordero-Llana O, Caldwell MA. 2017. Astrocytes in a dish: Using pluripotent stem cells to model neurodegenerative and neurodevelopmental disorders. *Brain Pathol* 27: 530-44

De Strooper B. 2007. Loss-of-function presenilin mutations in Alzheimer disease. Talking Point on the role of presenilin mutations in Alzheimer disease. *EMBO Rep* 8: 141-6

Elsworthy RJ, Aldred S. 2019. Depression in Alzheimer's Disease: An Alternative Role for Selective Serotonin Reuptake Inhibitors? *J Alzheimers Dis* 69: 651-61

Frommelt P, Schnabel R, Kühne W, Nee LE, Polinsky RJ. 1991. Familial Alzheimer disease: a large, multigeneration German kindred. *Alzheimer Dis Assoc Disord* 5: 36-43

Godbolt AK, Beck JA, Collinge J, Garrard P, Warren JD, et al. 2004. A presenilin 1 R278I mutation presenting with language impairment. *Neurology* 63: 1702-4

Gunhanlar N, Shpak G, van der Kroeg M, Gouty-Colomer LA, Munshi ST, et al. 2018. A simplified protocol for differentiation of electrophysiologically mature neuronal networks from human induced pluripotent stem cells. *Mol Psychiatry* 23: 1336-44

Hansson O, Lehmann S, Otto M, Zetterberg H, Lewczuk P. 2019. Advantages and disadvantages of the use of the CSF Amyloid β (Aβ) 42/40 ratio in the diagnosis of Alzheimer's Disease. *Alzheimers Res Ther* 11: 34

Hill E, Nagel D, Parri R, Coleman M. 2016. Stem cell-derived astrocytes: are they physiologically credible? *J Physiol* 594: 6595-606

Hoffmann J, Twiesselmann C, Kummer MP, Romagnoli P, Herzog V. 2000. A possible role for the Alzheimer amyloid precursor protein in the regulation of epidermal basal cell proliferation. *Eur J Cell Biol* 79: 905-14

Hossini AM, Megges M, Prigione A, Lichtner B, Toliat MR, et al. 2015. Induced pluripotent stem cell-derived neuronal cells from a sporadic Alzheimer's disease donor as a model for investigating AD-associated gene regulatory networks. *BMC Genomics* 16: 84

Israel MA, Yuan SH, Bardy C, Reyna SM, Mu Y, et al. 2012. Probing sporadic and familial Alzheimer's disease using induced pluripotent stem cells. *Nature* 482: 216-20

Kelleher RJ, Shen J. 2017. Presenilin-1 mutations and Alzheimer's disease. *Proc Natl Acad Sci U S A* 114: 629-31

Kondo T, Asai M, Tsukita K, Kutoku Y, Ohsawa Y, et al. 2013. Modeling Alzheimer's disease with iPSCs reveals stress phenotypes associated with intracellular Aβ and differential drug responsiveness. *Cell Stem Cell* 12: 487-96

Kuhn PH, Wang H, Dislich B, Colombo A, Zeitschel U, et al. 2010. ADAM10 is the physiologically relevant, constitutive alpha-secretase of the amyloid precursor protein in primary neurons. *EMBO J* 29: 3020-32

Kwart D, Gregg A, Scheckel C, Murphy E, Paquet D, et al. 2019. A Large Panel of Isogenic APP and PSEN1 Mutant Human iPSC Neurons Reveals Shared Endosomal Abnormalities Mediated by APP β-CTFs, Not Aβ. *Neuron* 104: 256-70.e5

Li T, Pires C, Nielsen TT, Waldemar G, Hjermind LE, et al. 2016a. Generation of induced pluripotent stem cells (iPSCs) from an Alzheimer's disease patient carrying a M146I mutation in PSEN1. *Stem Cell Res* 16: 334-7

Li T, Pires C, Nielsen TT, Waldemar G, Hjermind LE, et al. 2016b. Generation of induced pluripotent stem cells (iPSCs) from an Alzheimer's disease patient carrying an A79V mutation in PSEN1. *Stem Cell Res* 16: 229-32

Lu P, Bai XC, Ma D, Xie T, Yan C, et al. 2014. Three-dimensional structure of human γ-secretase. *Nature* 512: 166-70

Nalivaeva NN, Turner AJ. 2019. Targeting amyloid clearance in Alzheimer's disease as a therapeutic strategy. *Br J Pharmacol* 176: 3447-63

O'Brien RJ, Wong PC. 2011. Amyloid precursor protein processing and Alzheimer's disease. *Annu Rev Neurosci* 34: 185-204

Ochalek A, Mihalik B, Avci HX, Chandrasekaran A, Téglási A, et al. 2017. Neurons derived from sporadic Alzheimer's disease iPSCs reveal elevated TAU hyperphosphorylation, increased amyloid levels, and GSK3B activation. *Alzheimers Res Ther* 9: 90

Oikawa N, Walter J. 2019. Presenilins and γ-Secretase in Membrane Proteostasis. *Cells* 8

Okita K, Matsumura Y, Sato Y, Okada A, Morizane A, et al. 2011. A more efficient method to generate integration-free human iPS cells. *Nat Methods* 8: 409-12

Oksanen M, Petersen AJ, Naumenko N, Puttonen K, Lehtonen Š, et al. 2017. PSEN1 Mutant iPSC-Derived Model Reveals Severe Astrocyte Pathology in Alzheimer's Disease. *Stem Cell Reports* 9: 1885-97

Pannee J, Portelius E, Minthon L, Gobom J, Andreasson U, et al. 2016. Reference measurement procedure for CSF amyloid beta (Aβ). *J Neurochem* 139: 651-58

Pires C, Schmid B, Petræus C, Poon A, Nimsanor N, et al. 2016. Generation of a gene-corrected isogenic control cell line from an Alzheimer's disease patient iPSC line carrying a A79V mutation in PSEN1. *Stem Cell Res* 17: 285-88

Poon A, Li T, Pires C, Nielsen TT, Nielsen JE, et al. 2016. Derivation of induced pluripotent stem cells from a familial Alzheimer's disease patient carrying the L282F mutation in presenilin 1. *Stem Cell Res* 17: 470-73

Potter R, Patterson BW, Elbert DL, Ovod V, Kasten T, et al. 2013. Increased in vivo amyloid-β42 production, exchange, and loss in presenilin mutation carriers. *Sci Transl Med* 5: 189ra77

Rodríguez-Arellano JJ, Parpura V, Zorec R, Verkhratsky A. 2016. Astrocytes in physiological aging and Alzheimer's disease. *Neuroscience* 323: 170-82

Ryan NS, Nicholas JM, Weston PSJ, Liang Y, Lashley T, et al. 2016. Clinical phenotype and genetic associations in autosomal dominant familial Alzheimer's disease: a case series. *Lancet Neurol* 15: 1326-35

Sarasija S, Norman KR. 2018. Role of Presenilin in Mitochondrial Oxidative Stress and Neurodegeneration in. *Antioxidants (Basel)* 7

Scheuner D, Eckman C, Jensen M, Song X, Citron M, et al. 1996. Secreted amyloid beta-protein similar to that in the senile plaques of Alzheimer's disease is increased in vivo by the presenilin 1 and 2 and APP mutations linked to familial Alzheimer's disease. *Nat Med* 2: 864-70

Selkoe DJ, Hardy J. 2016. The amyloid hypothesis of Alzheimer's disease at 25 years. *EMBO Mol Med* 8: 595-608

Shi Y, Kirwan P, Livesey FJ. 2012. Directed differentiation of human pluripotent stem cells to cerebral cortex neurons and neural networks. *Nat Protoc* 7: 1836-46

Smith PK, Krohn RI, Hermanson GT, Mallia AK, Gartner FH, et al. 1985. Measurement of protein using bicinchoninic acid. *Anal Biochem* 150: 76-85

Sproul AA, Jacob S, Pre D, Kim SH, Nestor MW, et al. 2014. Characterization and molecular profiling of PSEN1 familial Alzheimer's disease iPSC-derived neural progenitors. *PLoS One* 9: e84547

Sun L, Zhou R, Yang G, Shi Y. 2017. Analysis of 138 pathogenic mutations in presenilin-1 on the in vitro production of Aβ42 and Aβ40 peptides by γ-secretase. *Proc Natl Acad Sci U S A* 114: E476-E85

Takahashi K, Yamanaka S. 2006. Induction of pluripotent stem cells from mouse embryonic and adult fibroblast cultures by defined factors. *Cell* 126: 663-76

Trombetta-Lima M, Sabogal-Guáqueta AM, Dolga AM. 2021. Mitochondrial dysfunction in neurodegenerative diseases: A focus on iPSC-derived neuronal models. *Cell Calcium* 94: 102362

Tubsuwan A, Pires C, Rasmussen MA, Schmid B, Nielsen JE, et al. 2016. Generation of induced pluripotent stem cells (iPSCs) from an Alzheimer's disease patient carrying a L150P mutation in PSEN-1. *Stem Cell Res* 16: 110-2

Wang X, Zhou X, Li G, Zhang Y, Wu Y, Song W. 2017. Modifications and Trafficking of APP in the Pathogenesis of Alzheimer's Disease. *Front Mol Neurosci* 10: 294

Weggen S, Beher D. 2012. Molecular consequences of amyloid precursor protein and presenilin mutations causing autosomal-dominant Alzheimer's disease. *Alzheimers Res Ther* 4: 9

Woodruff G, Young JE, Martinez FJ, Buen F, Gore A, et al. 2013. The presenilin-1 ΔE9 mutation results in reduced γ-secretase activity, but not total loss of PS1 function, in isogenic human stem cells. *Cell Rep* 5: 974-85

Xia D, Watanabe H, Wu B, Lee SH, Li Y, et al. 2015. Presenilin-1 knockin mice reveal loss-of-function mechanism for familial Alzheimer's disease. *Neuron* 85: 967-81

Yang J, Zhao H, Ma Y, Shi G, Song J, et al. 2017. Early pathogenic event of Alzheimer's disease documented in iPSCs from patients with PSEN1 mutations. *Oncotarget* 8: 7900-13

Zoltowska KM, Maesako M, Berezovska O. 2016. Interrelationship between Changes in the Amyloid β 42/40 Ratio and Presenilin 1 Conformation. *Mol Med* 22: 329-37